Assembling graphene aerogel hollow fibres for solar steam generation

Guangyong Li[1], Dan Fang[1], Guo Hong[2], Alexander Eychmüller[3], Xuetong Zhang[1,4,*], Wenhui Song[4,*]

[1] Suzhou Institute of Nano-Tech and Nano-Bionics, Chinese Academy of Sciences, Suzhou, 215123, P.R. China.

[2] Institute of Applied Physics and Materials Engineering, University of Macau, Macao.

[3] Physical Chemistry, Technische Universität Dresden, Bergstrasse 66b, Dresden 01062, Germany.

[4] Centre for Biomaterials in Surgical Reconstruction and Regeneration, Division of Surgery and Interventional Science, University College London NW3 2PF, United Kingdom.

[*] Corresponding author. E-mails: Xuetong Zhang, xtzhang2013@sinano.ac.cn or xuetong.zhang@ucl.ac.uk Wenhui Song, w.song@ucl.ac.uk

Highlights

- The GAHFs, consisted of cylindrical tube together with circular graphene aerogel wall, were fabricated for the first time by co-axial dynamic sol-gel spinning of graphene oxide liquid crystals with subsequent reduction and supercritical drying。

- An aligned GAHF array based solar steam generation system with exceptional high efficiency for water evaporation and salt rejection under 1.0 sun irradiation was developed.

- The GAHF roll based solar steam generation system expedited remarkable transpiration, reaching a record high water evaporation rate of ~3.29 kg m^{-2} h^{-1} under 1.0 sun solar radiation with outstanding salt-rejection performance, among the best evaporator reported in the literature.

TOC
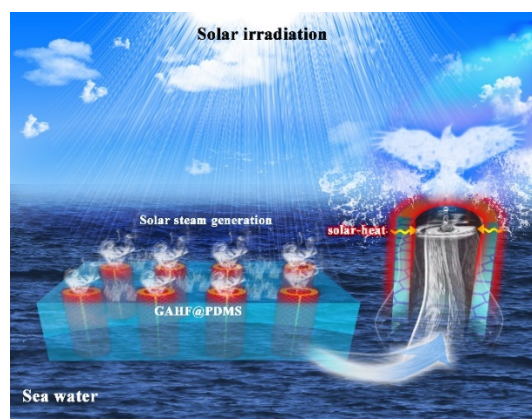
Abstract

Solar vapor generation, a cost-effective way to harvest solar energy for purifying polluted or saline water, has attracted great attention in recent years. However, during the harsh environment (e.g. high-salinity brine), challenges still remain in limited water evaporation, complicated/compromised systems between water transport, evapor area and salt accumulation. Herein, graphene aerogel hollow fibers (GAHF) are developed and assembled into a solar steam generator which demonstrates exceptionally high efficiency for water evaporation and salt rejection under sun irradiation. Inspired from the capillary water transportation system in trees, the mesophase-ordered GAHFs are spun from their liquid crystalline suspension, and subsequently assembled into a roll of unidirectionally aligned bundles and then embedded in a transparent polydimethylsiloxane (PDMS) matrix. The synergistic effects between GAHFs, serving as 1D-confining micro-channels for water transport and broadband solar absorbers, and PDMS matrix, as an light refractor and "canyons"-like evaporation area, improve the water flow and absorption of solar energy and maximize the evaporation surface area. As a result, the GAHF arrays expedite remarkable transpiration, achieving continuous steam generation (~3.29 kg m^{-2} h^{-1}) and outstanding salt-rejection performance for high-salinity brine (e.g. saturated solution) desalination. This GAHF based solar steam generation system provides a facile and high-performance device for self-generating seawater desalination.

Keywords Graphene aerogel, Hollow fibre, Solar steam generator, Desalination

1. Introduction

Solar energy is well known as a major source of renewable energy with the potential to meet the energy demand and to support the sustainable development of the world via various solar energy based techniques, such as the production of hydrogen, photovoltaic cells, photocatalysis, water purification, and water desalination [1, 2]. Among these techniques, solar-driven steam generation based on photo-to-thermal conversion is one of the most promising and efficient applications because freshwater could be directly produced from polluted or saline water[2, 3]. However, due to the poor light absorption of water and intensive heat losses, the natural light-to-vapor conversion efficiency is too low (< 20%) to generate a practical amount of fresh water. Hence, an advanced solar steam generation system with high light-to-heat conversion efficiency and excellent vapor generation performance has been in longing demand.

Interfacial evaporation system [4], in which the solar energy harvesting and steam generation were localized at the water-air interface, was successfully demonstrated with an improved efficiency of solar vapor generation based on the integration of the following key components: a multifunctional solar absorber, water transport and evaporation paths, and a thermal insulator. However, for most of previous evaporators [4, 5], the interfacial energy input and vapor generation occurred in the same interface, and the steam generation rates of these evaporators were pushed to the upper limit. To overcome the upper limit of vapor out, the 3D evaporator system was further designed via various strategies, such as enlarging evaporation area [6], extracting energy from bulk water [7-8], or eliminating energy loss and maximizing

energy gain from the surrounding environment [9]. Benefited from above strategies, the water evaporation rate broke the upper limit and reached to ~2.63 kg m^{-2} h^{-1} for 3D biomimetic evaporator [6], and ~4.19 kg m^{-2} h^{-1} for heatsink inspired solar evaporator [9]. Despite these improvements, the configurations of the components are complex with outstanding issues of further integration and requirement of more raw materials, and the aligned vessel channels for water transport and anti-fouling usually were sacrificed, which restrained long-term stability against a harsh environment. Therefore, the design and architecture of the current solar vapor generators are still far from ideal for solar steam generation with high efficient and long-term stability.

Graphene aerogels (GAs), 3D highly interconnected porous networks of graphene 2D nanosheets at macroscale, serving as a classic aerogel materials, have attracted great attentions in solar energy utilization, especially in steam generation, due to their outstanding broadband absorption for light-heat conversion, high porosity, wicking framework for water transport and evaporation, and others [10-14]. For the practical applications of GAs in solar steam generation, various structures and functions were designed and developed by specific strategies, such as 3D cross-linked honeycomb structure [12], the self-floating and hydrophilic GA [10], etc. However, most of the previous GA materials usually suffered from poor integration capability and machinable. GAs synthesised by the traditional static sol-gel process were produced only in simple macroscopic monolith shapes [15-17] and difficult to further process into a wide range of components with other integrative structures (e.g. combination of hollow channel, defined interior cavities, fiber-shape or others), which limited their applications into complex and

5

integrated systems [16]. Therefore, it is still challenging to develop an advanced and facile design and manufacturing strategy to produce versatile GA materials that can further assemble into a variety of architectures with desired functions.

Herein, graphene aerogel hollow fibres (GAHFs), serve as one novel architecture of GA that consisting of an aligned hollow channel and a porous aerogel wall, were fabricated for the first time by dynamic sol-gel co-axial spinning of graphene oxide liquid crystals (GO-LCs) with subsequent reduction and supercritical drying. Based on GAHF, a solar steam system with super high efficiency and excellent salt rejection was developed by embedding parallelly GAHFs embedded into a polydimethylsiloxane elastomer matrix (GAHF@PDMS), and a remarkable water transpiration (~3.29 kg m^{-2} h^{-1}) under 1.0 sun solar radiation with excellent stability and durability was achieved. Furthermore, the GAHF also exhibited a unique salt-rejecting behavior, which ensured the excellent and enduring solar steam generation in sea water desalination.

2. Results and Discussion

2.1. Fabrication and characterization of the GAHF and GAHF@PDMS

Water steam system based on GAHFs was developed through two stages, as shown in Scheme 1, from the fabrication of GAHFs (Scheme 1a) to the embedment of GAHFs in PDMS elastomer (Scheme 1b). In a typical fabrication process, the co-axial wet-spinning method[18] was adapted to produce GO hydrogel hollow fibres (GOHHFs), the colorful birefringent optical texture of liquid crystals under a cross-polarized-light microscope (Fig. 1a1-2 and Fig. S1) was

observed. After chemical reduction[18] and supercritical drying, the black GAHFs (Fig. S1) was obtained. The scanning electron microscopic (SEM) images (Fig. 1b-c and Fig. S2-3) show the circular hollow tubular structure of the GAHFs with a straight channel and thin annular aerogel wall. The diameter of the hollow channels were readily varied in range of 200-800 μm by changing the diameter of needles (Fig. S2-3). Consequently, the unidirectional GAHFs were woven into a tape and rolled up into a disc-like roll with the fibres aligned vertically. Finally, GAHF roll was embedded in PDMS resin and cured into a composite disc, followed by cutting and plasma O$_2$ treatment, obtaining the GAHF@PDMS, which is ready for use as a solar steam generator (Scheme 1c).
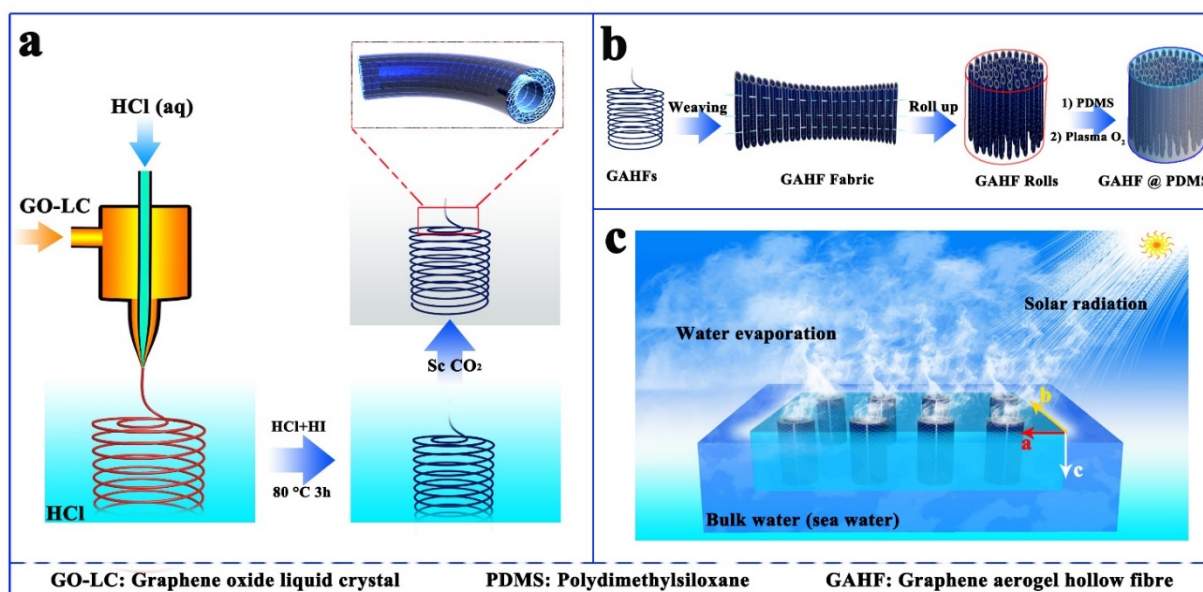
Scheme 1. The illustration of GAHF based solar vapor generation. (a) The fabrication of GAHF via co-axial wet-spinning, post reduction and supercritical drying. (b) The fabrication of GAHF@PDMS cylindrical pillars. (c) The schematic diagram of the GAHF@PDMS solar vapor generation system.

From the cross-section of GAHFs (Fig. 1c and Fig. S2-3), graphene sheets were packed more-or-less parallel to the circumferential orientation of tubular wall, with a large number of pores in a few hundred nanometers to a few microns aligned along the fibre axis. The isotherm (Fig. 1g) of as-prepared GAHF possessed a rapid increase in low-pressure range (P/P_0<0.02) and a hysteresis loop, which implied the existence of micro-pores and meso-pores in the as-prepared GAHF. After treated by Plasma-O_2, many oxygen-containing groups were introduced onto GAHF (Fig. S5-7), the plasma-O_2-treated-GAHF has also possessed micro-pores (0.35-0.67 nm), mesopores (3.5-44.1 nm), and the specific surface area was ~354 m^2 g^{-1}.

The as-prepared-GAHFs possessed a remarkable compliance with excellent mechanical properties (Fig. S8-9) [14, 19], which could be either tied into a knot without collapse (Fig. 1d), or woven into fabrics (Fig. 1e-f and Fig. S10), or rolled up into a cylinder-like roll (Fig. 1f1-f2). As GAHFs were packed into a unidirectional array within the PDMS matrix (inset in Fig. 1h), the regular round holes and porous annulus walls of GAHFs were well retained (Fig. 1h-i) and a long-range channel and porous thin-walls along axis of GAHF were observed (Fig. 1j). The percentage of GAHFs in composite roll could be tuned in the range of 8.0-35 vol.%.
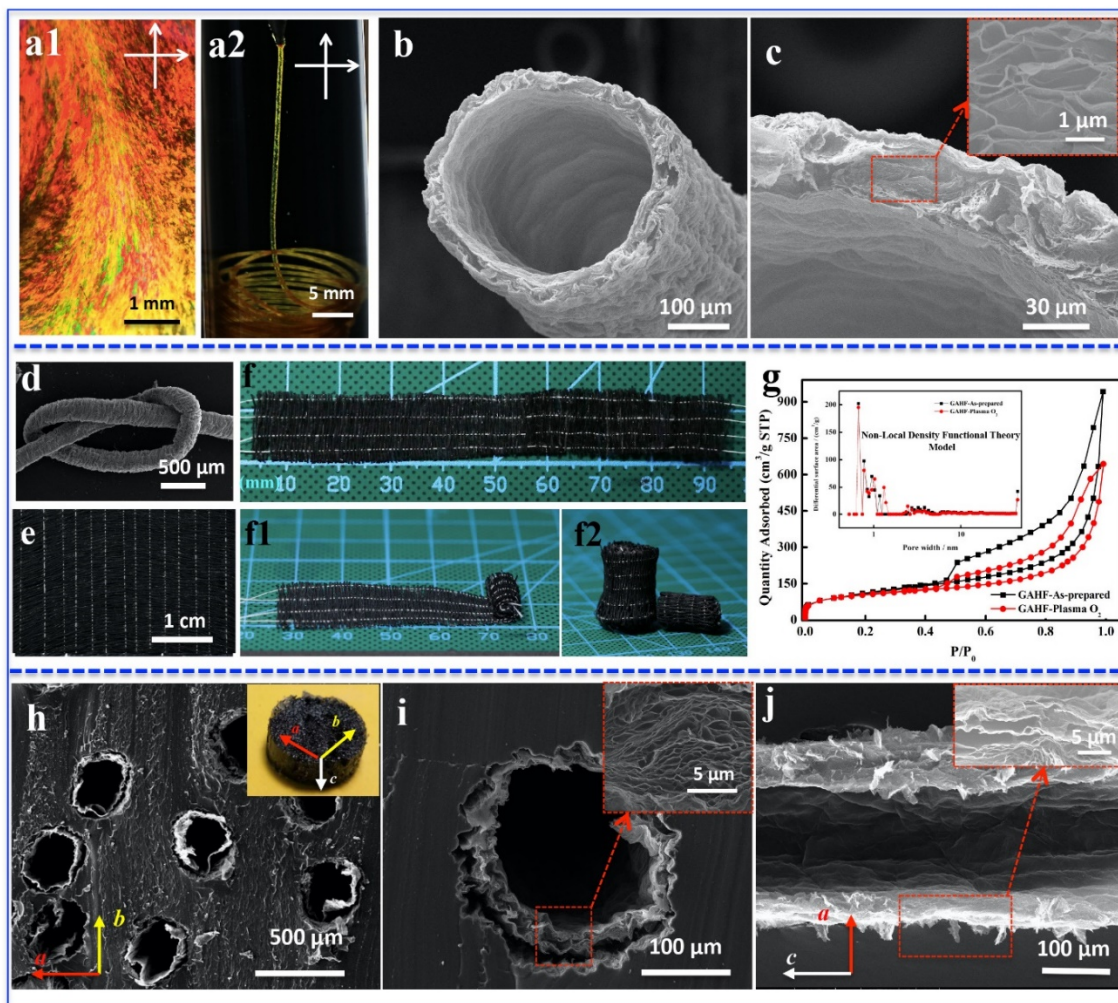
Fig. 1. Cross polarized-light optical images of GO-LC (a1) and GOHHF (a2). (b-d) SEM images of GAHFs. (e-f) Photographs of unidirectionally woven fabric, fabric tape and rolls of GAHFs. **g** The nitrogen sorption and pore size distribution curves of as-prepared GAHF and plasma-O_2-treated-GAHF. (h-j) SEM images of GAHF@PDMS composite. Inset in image (h) is the photograph of GAHF@PDMS, insets in image (c, i, j) are the corresponding close-up SEM images.

2.2. Fluid transport of GAHF@PDMS

The preliminary water-injection tests of single GAHF have been investigated and the results demonstrated that water could flow easily through the micro-channel under an external pressure (Fig. 2a and Fig. S11-14) [20-23]. However, GAHFs exhibited relatively weak hydrophilic behaviour with a static water contact angle (WCA) of ~60° (Fig. 2b) and the PDMS was relatively strong hydrophobic (~125°, Fig. S15). After an O_2-plasma treatment, the hydrophilic surfaces of GAHF and GAHF@PDMS were improved with a WCA of <20° (Fig. 2b) and ~0° (Fig. S15) respectively, which substantially improved the water wetting/absorbing and transport.

Water transport in GAHFs was evaluated by dynamic analysis of their sucking ability [24]. As shown in Fig. 2c and Fig. S17, the sucking process reached a saturated status in a few seconds, indicating a faster water transport than other evaporators [24, 25]. The plasma-O_2-treated-GAHFs processed about two times higher saturated water content (23 g g^{-1}) than that of as-prepared-GAHFs (~12 g g^{-1}). The aerogel wall of GAHF as a wicking structure, generating additional capillary force, larger than the hollow channels, which could speed up the water transportation between the hollow channel and the aerogel wall (Fig. S18). When the paper contacted the surface of GAHF@PDMS vertically, magenta ink appeared to diffuse into paper in a few seconds (Fig. 2d). The synergistic effect between hollow channel and aerogel wall at multiscale rendered the fast water transport behaviour (Fig. 2e).

2.3. Solar-thermal effect of GAHF@PDMS

GAHF@PDMS remained in a black appearance in the presence of a dense array of GAHFs, as well as inherited efficient broadband solar absorption (97.3-98.1%, Fig. 2f) [26]. When solar

irradiation was parallel to the axial direction of GAHFs, a uniform temperature distribution (inset in Fig. 2f) and a confined effect of thermal absorption (Fig. S19) were observed clearly on the top-cross-section of GAHF@PDMS in the air according to infrared (IR) images. As shown in Fig. 2g and Fig. S20, the temperature of the top surface of GAHFs increased exponentially under solar irradiation, which exhibited the highest increase rate and temperature as compared to the other locations of GAHF@PDMS, in evidence of the effective energy confinement within the GAHFs.

Furthermore, as the single-layer GAHF fabric was embedded into PDMS, the irradiation was parallel to axial direction of GAHFs (Fig. 2h-j), both the top-section and side-surface of GAHF@PDMS exhibited a uniform temperature distribution (Fig. 2k). This indicated that the light could pass through the transparent PDMS matrix [27-28]. Radiated light direction was changed at the interface between air and PDMS via refraction (Fig. 2h) on the rough surface of PDMS (Fig. 2l-n and Fig. S21), resulting in that the outside-wall-surface of GAHF could receive irradiation energy and irradiation energy absorbed by outside-wall-surface of GAHF could transfer to inside-wall-surface of GAHF (Fig. S22). Aerogel structure along the axial direction of GAHF could suppress the thermal energy loss (Fig. S23), similar to aerogel based water evaporation system [12].
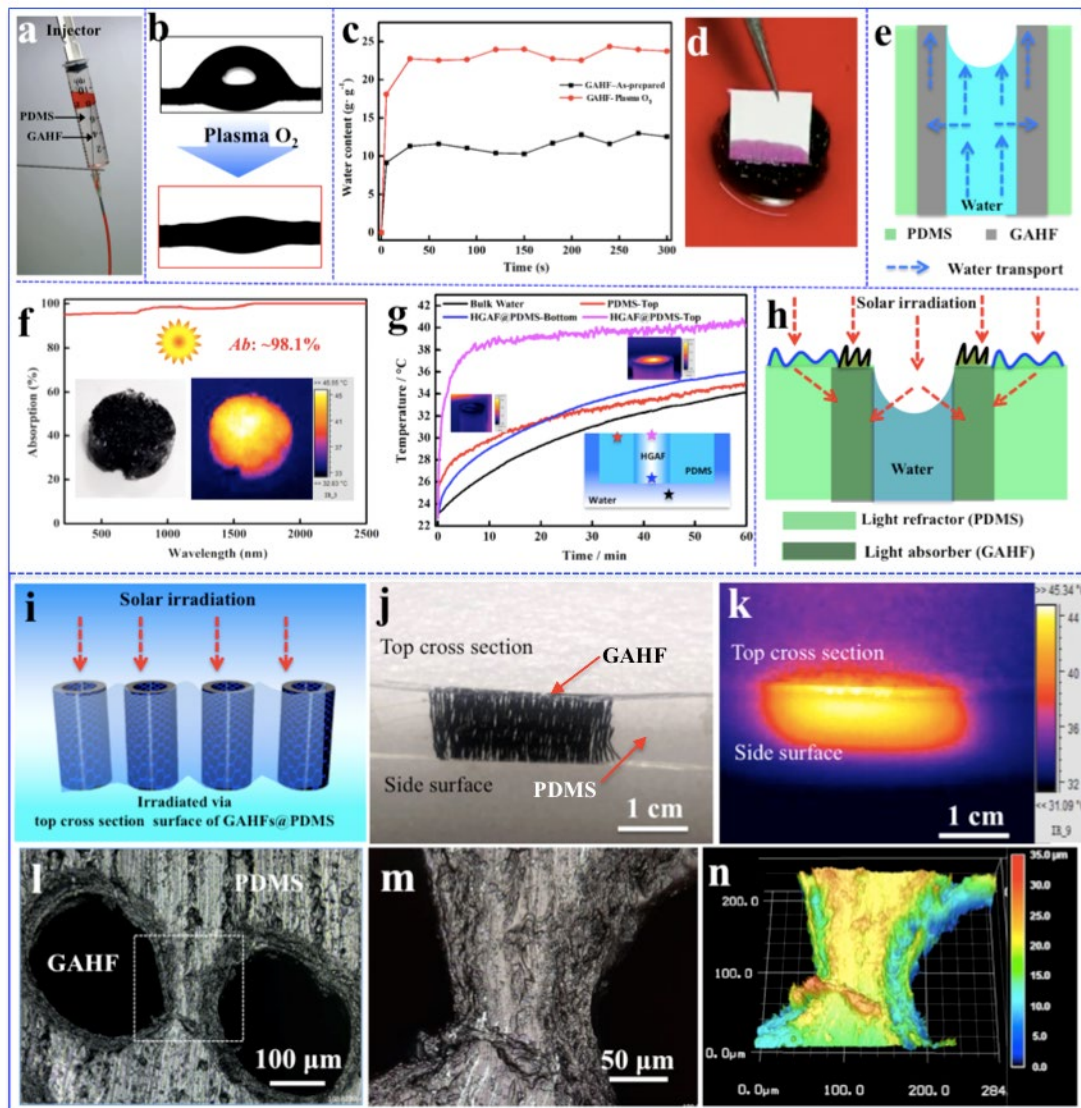
Fig. 2. The water transport and light-to-heat conversion of GAHFs and GAHF@PDMS. (a) Photograph of GAHF@PDMS in one injector. The water contact angles (b), sucking process **(c)** of as-prepared GAHFs and plasma-O_2-treated-GAHFs. (d) Photograph of white paper wicking magenta-ink underneath GAHF@PDMS. (e) Illustration of water transport in GAHF@PDMS. (f) UV-vis-NIR spectra of GAHF@PDMS. (g)Temperature-time curves of the different positions of GAHF@PDMS under 1.0 sun. (h) Illustration of the light propagation at interface between air and rough PDMS surface. (i-k) Images of single-layer GAHF@PDMS

under 1.0 sun. (l-n) Morphological images of GAHF@PDMS via 3D confocal microscopy. Insets of (f-g) are photograph and IR image of GAHF@PDMS.

2.4. Solar vapor generation under 1.0 sun

Water evaporation properties was recorded under constant solar illumination (1 kW m^{-2}), environmental temperature was 25±2 °C and relative humidity was 45±3% [29], and GAHF@PDMS self-floats on water surface. It has been found that each GAHF works alone and there are no obvious mutual interferences among each other (Fig. S24). GAHF@PDMS presented an extraordinarily high mass change rate of ~3.29 kg m^{-2} h^{-1} (Equation S1), which was 11 times higher than that from pure water (Fig. 3a-c and Fig. S25-26), higher than most previous reports (Table S1). In addition, as the diameter and number of GAHF@PDMS increased (e.g., assembling four GAHF@PDMS samples together into one evaporator), GAHF@PDMS evaporator still exhibited a high vapor of 2.99±0.21 kg m^{-2} h^{-1} (Fig. S27).

When solar irradiation was removed (Fig. 3a-b), GAHFs@PDMS still remained water evaporation rate at 0.85 kg m^{-2} h^{-1}, higher than that of pure water under light off field (~0.13 kg m^{-2} h^{-1}), and comparable to the bio-mimetic 3D solar evaporator (~0.84 kg m^{-2} h^{-1}) [6]. According to DSC curves (Fig. S28), water evaporation onset temperature was down-shifted from 72 °C for pure water to to 51 °C for water in GAHFs. In addition, the equivalent water vaporization enthalpy of water in GAHF@PDMS was measured by dark evaporation experiments [24, 30], which was ~851 J/g. Hence, the combination of GAHF and PDMS has played a synergetic role for the high water evaporation rate.

The functions of porous walls and hollow channels under water vapor production were investigated, in comparison with graphene hollow fibres (GHF, no aerogel wall) and graphene aerogel fibre (GAF, no hollow channel) (Fig. 3d and Fig. S29). Water evaporation rate of GAHF@PDMS is 1.2 higher than that of GHF@PDMS (2.67 kg m^{-2} h^{-1}) and 8 times higher than that of GAF@PDMS (0.38 kg m^{-2} h^{-1}). When the diameter of hollow channels was increased, the water evaporation rate was reduced sharply (Fig. S30). These results indicated the prodominant contribution from the hollow channels of GAHFs.

According to COMOSL simulation (S2.3), the steady-state temperature distribution predicated that the maximum temperature was confined to the top-cross-section of GAHF@PDMS (Fig. 3e and Fig. S31). Additionally, the 2D mapping of water velocity distribution depicted a faster water transport through hollow channels than through aerogel walls (Fig. 3f), in agreement with the above analysis given by Hagen-Poiseuille law (S2.4).

According to the above results, the synergistic effect between the integrative GAHFs and PDMS improves the solar absorption, external environment energy input and vapor evaporate area. GAHFs serve as integrative solar absorber (Fig. 3g) and multi-scale water transport channel (Fig. 3i), and transparent PDMS serves as light refractor and enlarged evaporation area ("canyons"-like topography). Under the solar irradiation, GAHFs worked like thousands of heated up "micro-tube-furnaces", the closed annulus wall could provide a thermal aggregation effect for the center cavity (Fig. 3g) [26], and thermal exchange among GAHFs occurred through PDMS (Fig. 3h). Under the capillary forces derived from GAHFs, bulk water was

pumped into GAHF, and the water could form a menisci surface in hollow channel of GAHF

and then spread quickly to the rough PDMS surface (Fig. 3i). The menisci of water-air interface

provides a vaporizing water area of about two times larger than the flat-plane-interface[30], and

the rough hydrophilic PDMS surface also further enlarges the effective water vaporizing area.
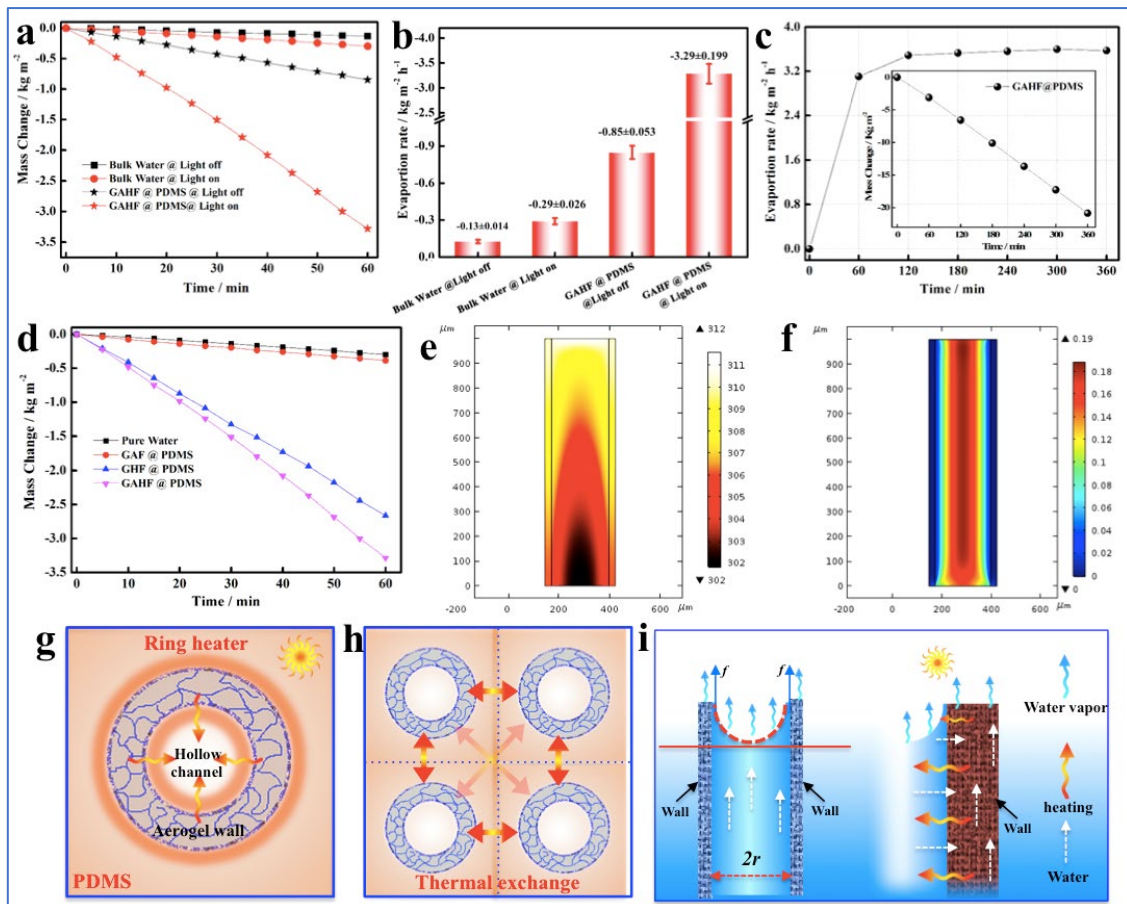
Fig. 3. The water evaporation of the GAHF based solar steam generation system. (a) The mass

loss of water and (b) evaporation rate values of GAHF@PDMS and pure water with or without

solar irradiation, each error bar represents the deviation from five data points, GAHF@PDMS:

height of 4-6 mm, diameter of 9-10 mm. GAHFs with outer diameter of 275 μm and wall

thickness of 25 μm. (c) The water mass change rate (with the inset of mass change) of

GAHF@PDMS during continuous exposure to 1.0 sun for 6 h. (d) The water mass loss of pure

water, GAHF@PDMS, GHF@PDMS and GAF@PDMS. Theoretical simulation of (e) temperature distribution and (f) water transport in GAHF@PDMS. The illustrations (g-i) of water evaporation model of GAHF.

2.5. Solar desalination and salt rejection

Water evaporation from the brine samples was investigated simulating salinity-Bohai sea (~3wt%) and a saturated solution (~26 wt%) (Fig. 4a-g). Compared with deionized water with an evaporation rate of ~3.29 kg m^{-2} h^{-1}, GAHF@PDMS also exhibited an excellent solar desalination behaviour with a high water vapor rate of ~2.94 kg m^{-2} h^{-1} for salinity-Bohai sea and ~2.08 kg m^{-2} h^{-1} for saturated salt water, respectively. GAHF@PDMS remained at a stable evaporation rate under continuous irradiation for 12 h, being promising for feasible long-term solar desalination.

The hollow channel and the aerogel wall of GAHFs could serve as a salt-rejection structure to prevent the salt accumulation under continuous operation. Various visible assumption experiments were carried out Fig. 4b-d and Fig. S32) to demonstrate the salt diffusion and rejection behaviour of composites [31]. CuCl$_2$, rhodamine B (RhB) and NaCl powders were dissolved and diffused back to bulk water within a few minutes (Fig. 4b-d, and Fig. S32), and the blue solution of Cu^{2+} and the violet line-current of RhB diffusion were observed, indicating that salt powder barely remained in evaporator and hollow channel could provide a micro-cycle of salt flux [31, 32] for advecting and diffusing the concentrated salt down back into bulk water (Fig. 4h).

Furthermore, the salt rejection behaviour was investigated on saturated solution (>26 wt% NaCl aq). After 8 h under 1.0 sun irradiation, white bulk crystals of NaCl around black holes was formed on the top surface of GAHF@PDMS (Fig. 4h and Fig. S33-35): black holes were surrounded by white salt crystals (Fig. 4f-g), and icicles of crystals on the bulk crystals were also observed, indicating most hollow channels were not blocked by salt crystals. In addition, the formed salt crystals could be wiped out easily for leaving a clean evaporation surface (Fig. S34).
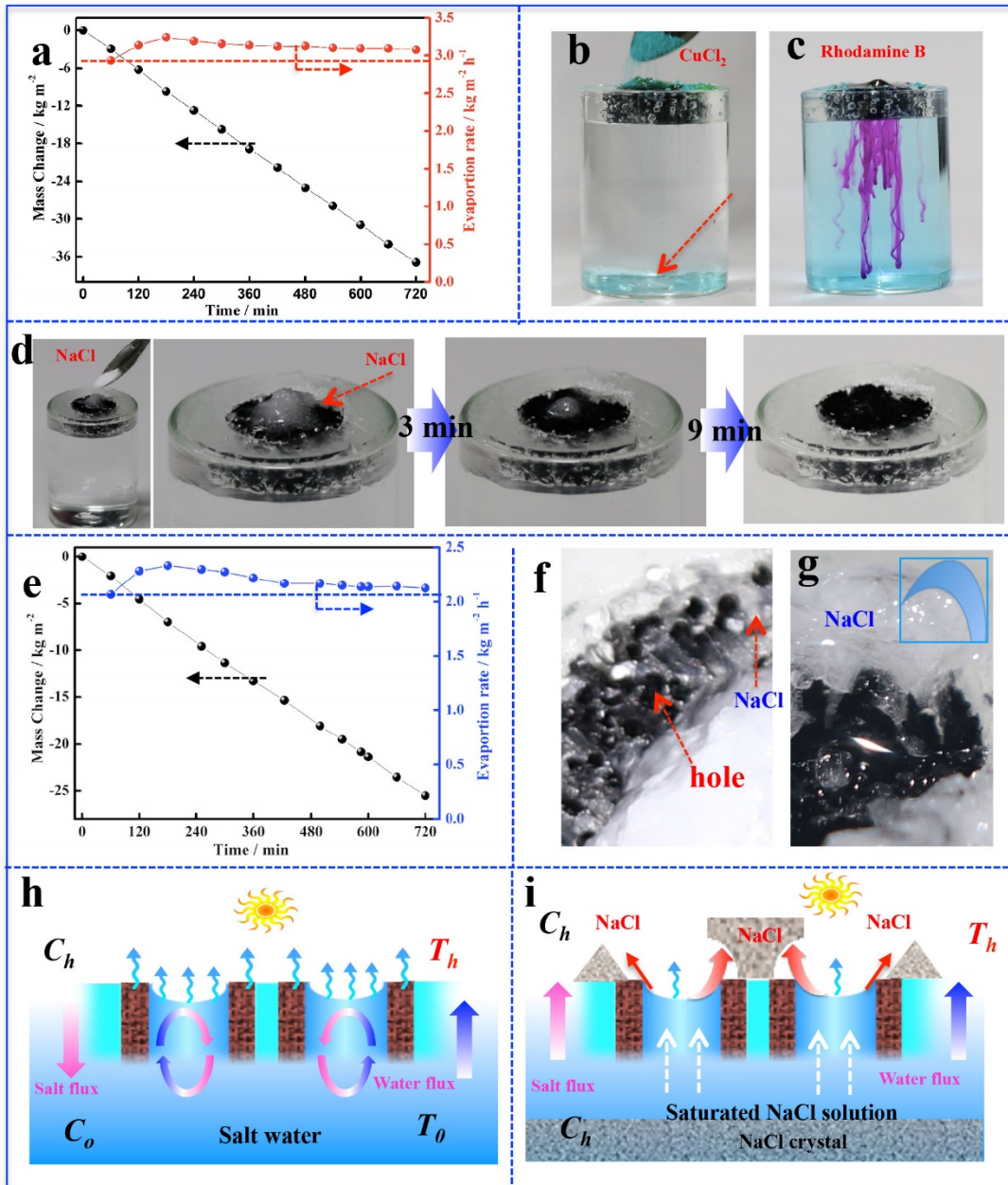
Fig. 4. The salt rejection behaviour of the GAHF based solar steam generation system. (a) The evaporation behaviour of a salt solution in simulated salinity-Bohai sea water (3%) and (b-d) the dissolution/diffusion behaviour of salt/dye on the top surface of GAHF@PDMS. (e) The evaporation behaviour and (f-g) crystallization of the saturated salt solution on the surface of GAHF@PDMS. The scheme of salt rejection on the HGAF@PDMS water evaporator for (h) low aqueous concentrations and (i) a saturated solution of the salt.

3. Conclusion

We demonstrated production of GAHFs and assembling them into macroscale composites for solar energy harvesting applications. A highly effecient solar steam generator was developed by rolling up GAHFs perpenticular to PDMS matrix. This evaporator provided a remarkable water transpiration under 1.0 sun solar irradiation. Furthermore, the GAHF@PDMS also exhibited excellent stability, durability and a unique salt-rejecting behaviour, which ensured excellent solar steam properties in sea water desalination. This work offers a new strategy of engineering assembling graphenes for a facile and cost-effective application in sea water desalination in the future.

Declaration of competing interest

The authors declare that they have no known competing financial interests or personal relationships that could have appeared to influence the work reported in this paper.

Acknowledgements

Appendix A. Supplementary data

Supplementary data related to this article can be found at .

References

[1] L. Zhu, M. Gao, C.K.N. Peh, G.W.W. Ho, Solar-driven photothermal nanostructured materials designs and prerequisites for evaporation and catalysis applications, Mater. Horiz., 5, (2018) 323-343.

[2] M. Gao, L. Zhu, C.K.N. Peh, G.W.W. Ho, Solar absorber material and system designs for photothermal water vaporization towards clean water and energy production, Energy Environ. Sci., 12, (2018) 841-864.

[3] G. Liu, J. Xu, K. Wang, Solar water evaporation by black photothermal sheets, Nano Energy, 41, (2017) 269-284 .

[4] P. Tao, G. Ni, C. Song, W. Shang, J. Wu, J. Zhu, G. Chen, T. Deng, Solar-driven interfacial evaporation, Nature Energy, 3, (2018) 1031-1041.

[5] Z. Deng, J. Zhou, M. Lei, C. Liu, S. Tanemura, The emergence of solar thermal utilization: Solar-driven steam generation, J. Mater. Chem. A, 5, (2017) 7691-7709.

[6] L. Wu, Z. Dong, Z. Cai, T. Ganapathy, N.X. Fang, C. Li, C. Yu, Y. Zhang, Y. Song, Highly efficient three-dimensional solar evaporator for high salinity desalination by localized crystallization, Nat. Commun., 11, (2020) 521.

[7] Y. Wang, X. Wu, X. Yang, G. Owens, H. Xu, Reversing heat conduction loss: Extracting energy from bulk water to enhance solar steam generation, Nano Energy, 78, (2020) 105269.

[8] Y. Wang, X. Wu, P. Wu, J. Zhao, X. Yang, G. Owens, H. Xu, Enhancing solar steam generation using a highly thermally conductive evaporator support, Sci. Bull., 66, (2021) 2479.

[9] X. Wu, Z. Wu, Y. Wang, T. Gao, Q. Li, H. Xu, All-cold evaporation under one sun with zero energy loss by using a heatsink inspired solar evaporator, Adv. Sci., 8, (2021) 2002501.

[10] Y. Fu, G. Wang, T. Mei, J. Li, J. Wang, X. Wang, Accessible graphene aerogel for efficiently harvesting solar energy, ACS Sustain. Chem. Engineer., 5, (2017) 4665-4671.

[11] P. Zhang, J. Li, L. Lv, Y. Zhao, L. Qu, Vertically aligned graphene sheets membrane for highly efficient solar thermal generation of clean water, ACS Nano, 11, (2017) 5087-5093.

[12] Y. Yang, R. Zhao, T. Zhang, K. Zhao, P. Xiao, Y. Ma, P.M. Ajayan, G. Shi, Y. Chen, Graphene-based standalone solar energy converter for water desalination and purification, ACS Nano, 12, (2018) 829-835.

[13] Y. Li, T. Gao, Z. Yang, C. Chen, Y. Kuang, J. Song, C. Jia, E.M. Hitz, B. Yang, L. Hu, Graphene oxide-based evaporator with one-dimensional water transport enabling high-efficiency solar desalination, Nano Energy, 41, (2017) 201-209.

[14] G. Li, G. Hong, D. Dong, W. Song, X. Zhang, Multiresponsive graphene-aerogel-directed phase-change smart fibers, Adv. Mater., 30, (2018) e1801754.

[15] X. Zhang, Z. Sui, B. Xu, S. Yue, Y. Luo, W. Zhan, B. Liu, Mechanically strong and highly conductive graphene aerogel and its use as electrodes for electrochemical power sources, J. Mater. Chem. A, 21, (2011) 6494-6497.

[16] G. Li, D. Dong, G. Hong, L. Yan, X. Zhang, W. Song, High-efficiency cryo-thermocells assembled with anisotropic holey graphene aerogel electrodes and a eutectic redox electrolyte, Adv. Mater., 31, (2019) 1901403.

[17] G. Li, X. Zhang, J. Wang, J. Fang, From anisotropic graphene aerogels to electron- and photo-driven phase change composites, J. Mater. Chem. A, 4, (2016) 17042-17049.

[18] Y. Zhao, C. Jiang, C. Hu, Z. Dong, J. Xue, Y. Meng, N. Zheng, P. Chen, L. Qu, Large-scale spinning assembly of neat, morphology-defined, graphene-based hollow fibers, ACS Nano, 7, (2013) 2406-2412.

[19] Z. Xu, Y. Zhang, P.G. Li, C. Gao, Strong, conductive, lightweight, neat graphene aerogel fibers with aligned pores, ACS Nano, 6, (2012) 7103-7113.

[20] K.P. Katuri, N.M. Bettahalli, X. Wang, G. Matar, S. Chisca, S.P. Nunes, P.E. Saikaly, A microfiltration polymer-based hollow-fiber cathode as a promising advanced material for simultaneous recovery of energy and water, Adv. Mater., 28, (2016) 9504.

[21] A. Akbari, P. Sheath, S.T. Martin, D.B. Shinde, M. Shaibani, P.C. Banerjee, R. Tkacz, D. Bhattacharyya, M. Majumder, Large-area graphene-based nanofiltration membranes by shear alignment of discotic nematic liquid crystals of graphene oxide, Nat. Commun., 7, (2016) 10891.

[22] K.H. Thebo, X. Qian, Q. Zhang, L. Chen, H.M. Cheng, W. Ren, Highly stable graphene-oxide-based membranes with superior permeability, Nat. Commun., 9, (2018) 1486.

[23] K. Goh, W. Jiang, H.E. Karahan, S. Zhai, L. Wei, D. Yu, A.G. Fane, R. Wang, Y. Chen, All-carbon nanoarchitectures as high-performance separation membranes with superior stability, Adv. Funct. Mater., 25, (2016) 7348.

[24] F. Zhao, X. Zhou, Y. Shi, X. Qian, M. Alexander, X. Zhao, S. Mendez, R. Yang, L. Qu, G. Yu, Highly efficient solar vapour generation via hierarchically nanostructured gels, Nat. Nanotech., 13, (2018) 489-495.

[25] X. Zhou, Z. Fei, Y. Guo, Z. Yi, G. Yu, A hydrogel-based antifouling solar evaporator for highly efficient water desalination, Energy Environ. Sci., 11, (2018) 1985-1992.

[26] M. Zhu, Y. Li, F. Chen, X. Zhu, H. Liangbing, Plasmonic wood for high-fficiency solar steam generation, Adv. Energy Mater., (2017) 1701028.

[27] L. Zhou, H. Song, J. Liang, M. Singer, M. Zhou, E. Stegenburgs, N. Zhang, C. Xu, T. Ng, Z. Yu, B. Ooi, Q. Gan, A polydimethylsiloxane-coated metal structure for all-day radiative cooling, Nature Sustain., 2, (2019) 718-724.

[28] P. Mellado, H.A. McIlwee, M.R. Badrossamay, J.A. Goss, L. Mahadevan, K. Kit Parker, A simple model for nanofiber formation by rotary jet-spinning, Appl. Phy. Lett., 99 (2011) 203107.

[29] T. Gao, X. Wu, Y. Wang, G. Owens, H. Xu, A hollow and compressible 3D photothermal evaporator for highly efficient solar steam generation without energy loss, Sol. RRL, 5, (2021) 2100053.

[30] Y. Lu, D. Fan, Z. Shen, H. Zhang, H. Xu, X. Yang, Design and performance boost of a mof-functionalized-wood solar evaporator through tuning the hydrogen-bonding interactions, Nano Energy, 95, (2022) 107016.

[31] T.D. Wheeler, A.D. Stroock, The transpiration of water at negative pressures in a synthetic tree, Nature, 455, (2008) 208-212.

[32] G.W. Ni, S.H. Zandavi, S.M. Javid, S.V. Boriskina, T.A. Cooper, C. Gang, A salt-rejecting floating solar still for low-cost desalination, Energy Environ. Sci., 11, (2018) 1510-1519.

[33] S. He, C. Chen, Y. Kuang, R. Mi, Y. Liu, Y. Pei, W. Kong, W. Gan, H. Xie, E. Hitz, Nature-inspired salt resistant bimodal porous solar evaporator for efficient and stable water desalination, Energy Environ. Sci., 12, (2019) 1558-1567.